Presented at the 32nd European PV Solar Energy Conference and Exhibition, 20-24 June 2016, Munich, Germany

COMPREHENSIVE STUDY OF INTERMETALLIC COMPOUNDS IN SOLAR CELL INTERCONNECTIONS INCLUDING LEAD-FREE, LOW MELTING POINT SOLDERS

Torsten Geipel[a], Monja Moeller[b], Achim Kraft[a], Ulrich Eitner[a]
[a] Fraunhofer Insitute for Solar Energy Systems ISE, 79110 Freiburg, Germany
[b] Kiel University, Institute of Material Science, 24098 Kiel, Germany

ABSTRACT: Intermetallic compounds (IMC) in solder bonds are commonly considered critical for the reliability of interconnections. The microstructure and thermal aging characteristics of solder bonds of crystalline silicon solar cells are investigated, whereby two solders, Sn60Pb40 and a lead-free, low melting point alternative Sn41Bi57Ag2 are considered. Solder bonds of front side busbars are formed with a semi-automatic tool and cross sections are prepared, which are characterized with confocal laser microscopy, scanning electron microscopy and energy dispersive x-ray spectroscopy (EDX). The kinetic of IMC growth is modeled with a diffusion model, and the parameters are obtained with systematic thermal aging studies and the Arrhenius relationship. The model is capable of processing non-isothermal temperature profiles and is used to simulate IMC growth during PV module reliability tests like thermal cycling 600 (TC) and damp heat for 3000 h. Furthermore, the thicknesses of the IMCs are estimated for a PV module in an outdoor location. It is found that solder joints undergo strong ripening processes during thermal aging. In particular, Sn41Bi57Ag2 solder joints show faster IMC growth, grain coarsening and Sn-penetration into the busbar than Sn60Pb40 bonds. Sn-penetration is observed already in the as-soldered condition and EDX confirms the existence of significant amounts of diffused Sn around cavities in the busbar. Large portions of the busbar are consumed by the Ag_3Sn IMC after 155 h at 130 °C and further aging of the Sn41Bi57Ag2 joint leads to Bi segregation and, in some cases, complete depletion of Sn from the solder matrix. The simulation of IMC growth shows a final IMC thickness after TC 600 of 1.2 µm and 1.5 µm; furthermore, a thickness after 3000 h at 85°C of 2.6 µm and 3.7 µm respectively for Ag_3Sn in Sn60Pb40 and Ag_3Sn in Sn41Bi57Ag2 bonds. The prognosis of IMC growth in a PV module in the outdoor location estimates an Ag_3Sn thickness of 1.2 µm and 1.3 µm for Sn60Pb40 and Sn41Bi57Ag2 respectively due to the rare occurrence of temperatures above 60 °C.

Keywords: PV Module, Module Integration, Metallization, Reliability

1 MOTIVATION, GOALS AND APPROACH

Reliability of PV modules directly impacts the levelized cost of electricity (LCOE) of PV systems [1]. The series interconnection of solar cells into strings via soldering, which is part of the module assembly process, determines the reliability of the final product in such a way that inappropriate soldering conditions or material selection damages solar cells during the process and subsequent aging [2–4]. Furthermore, fatigue, coarsening as well as voiding in solder bonds are commonly observed failure modes in field-aged PV modules [5–7]. In order to more efficiently prevent such solder bond failures in PV modules this work intends to increase the understanding of thermal aging phenomena in solder bonds with a focus on intermetallic compounds (IMC).

IMCs are typically considered critical because of their brittleness and resulting inability to withstand thermomechanical fatigue [8]. The goals are to describe microstructural changes during thermal aging, to quantify the IMC growth and to simulate it under various aging conditions. Not only a standard lead-based solder alloy is considered in the investigation but also a lead-free, bismuth-based low melting point solder, that may be of relevance for the interconnection of temperature-sensitive heterojunction solar cells [9]. A direct comparison between the standard solder and the low-melting point solder is to be made.

The approach is to solder interconnector ribbons on the front side busbars of solar cells, which are then processed into metallographic cross sections. Those are characterized in terms of solder and IMC microstructure. Then, the cross section samples are isothermally aged at various temperatures and time steps. Subsequently, the measurement of the IMC growth at different temperatures allows the extraction of the kinetic parameters of an IMC growth model. Eventually, the model is used to make predictions during accelerated aging and under outdoor conditions.

2 MATERIALS AND METHODS

2.1 Solder bonds and solder materials

Soldering is the metallurgical joining of two or more substrates using an interjacent material (solder), which is able to melt and solidify at significantly lower temperatures than the substrates [10]. The process of soldering involves heating of the substrates and the solder, the removal of oxides and the activation of the substrates' surfaces with the flux and passing the melting temperature of the solder, which then is able to wet and spread on the substrates. Thin layers of the substrates are dissolved in the molten solder, and the molten alloy with the foreign atoms near the interface subsequently leads to the formation of intermetallic layers [11]. The microstructure obtained after solidification is strongly influenced by the cooling dynamics. The initial structure changes during thermal aging and even storage at room temperature. The microstructure determines the mechanical properties of the bond [12].

Thin and uniform intermetallic layers are an indication for a good metallurgical bond [11]. These layers tend to grow temperature driven and, due to their brittleness, reduce the fatigue resistance of the bonds [8,13–15]. Possible intermetallic compounds, their stoichimetry and elemental compositions are displayed in the respective alloy's phase diagram [16,17].

Table I. Ribbon material, alloy coatings and processing conditions.

	Sn60Pb40	Sn41Bi57Ag2
Ribbon dimensions [mm × mm]	1.5 × 0.2	1.5 × 0.18
Solder coating thickness [µm]	15 – 25	15 – 25
Solder melting temperature [°C]	183 – 187 °C	139 °C
Set soldering temperature [°C]	250	200
Set heating chuck temperature [°C]	175	135
Soldering time [s]	1.2	1.2
Downholding time [s]	4	4

The tin-lead alloy with the eutectic or near-eutectic compositions of 63 wt.% Sn and 37 wt.% Pb or 60 wt.% Sn and 40 wt.% Pb (Sn60Pb40) is mostly used in today's PV module manufacturing. Although Pb is a toxic material, banned by the European Parliament from many electronic products through the RoHS legislation [18], SnPb solder has many advantages in terms of its relatively low melting point of 183 °C, low cost, superior wetting behaviour and outstanding ductility, that easily absorbs thermomechanical stress [14].

Alloys based on tin-bismuth are considered as replacement to reduce thermomechanical stress during the soldering process of thin solar cells or for the interconnection of temperature-sensitive solar cells [19,20]. They are often used in the eutectic composition of 43 wt.% Sn and 57 wt.% Bi. A minor addition of Ag improves the mechanical properties of the alloy by refining its microstructure [21,22]. In this work Sn41Bi57Ag2 is used. The alloy has a melting temperature of 139 °C, the benefits of costs lower than indium-tin alloys, and it is a lead-free material. Bismuth is often deemed disadvantageous with regard to segregation, brittleness, fatigue life, the high homologous temperature at operation and negative thermal expansion during the melting/solidification phase transition [23–27]. However, not all researches find negative effects on joint strength before or after aging [28,29], which means that the situation is more complex and SnBi(Ag) has the potential to complement SnPb in specific applications.

2.2 Modeling of intermetallic phase growth

The growth of intermetallic phases during thermal aging is considered to be a diffusion-driven process. If a random walk treatment of Fick's second law is made, the mean square diffusion distance of atoms during solid state aging $\bar{x}^2$ in one dimension is expressed with equation 1 [30].

$$\bar{x}^2 = 2Dt \tag{1}$$

Hereby, D stands for the temperature dependent diffusion coefficient and t for the time of thermal aging.
The diffusion coefficient is typically described by the Arrhenius relationship:

$$D = D_0 \exp\left(-\frac{Q}{RT}\right) \tag{2}$$

D_0 is the pre-exponential factor, Q is the activation energy of the growth process, R is the gas constant and T is the absolute temperature. Combining equations (1) and (2) yields to the intermetallic layer thickness x after thermal aging:

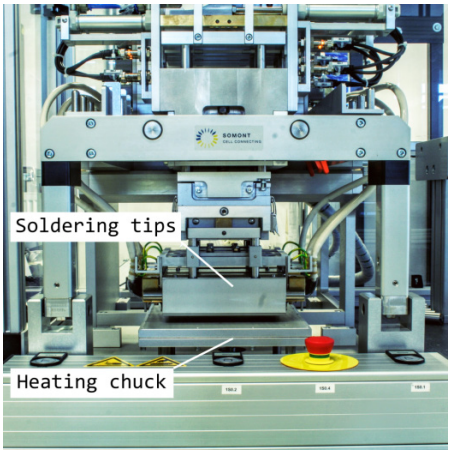

Figure 1. Semi-automatic soldering station.

$$x = \sqrt{2D_0 t \exp\left(-\frac{Q}{RT}\right)} + x_0 \tag{3}$$

with x_0 as the initial IMC thickness.

In order to make predictions of the intermetallic layer thickness, equation 3 requires the parameters D_0, Q and x_0 as an input, which are obtained by systematically measuring the IMC thickness at different temperatures and constant time intervals. Having those, the natural logarithm is taken of equation 3, and a rearrangement leads to a linear relationship between $\ln(x–x_0)$ and $1/T$ as shown in equation 4.

$$\ln(x - x_0) = \frac{\ln(2D_0 t)}{2} - \frac{Q}{2R}\frac{1}{T} \tag{4}$$

The slope of equation 4 gives the activation energy. Further non-linear fitting of the experimental data of thickness x to equation 3 with t as the dependent variable and Q, T, x_0 as constant parameters eventually leads to the extraction of D_0.

As equation 3 only allows predictions for a constant temperature, a numerical solving routine is necessary if non-isothermal conditions are considered.

2.3 Sample preparation and characterization

Copper ribbons with two different solder coatings, Sn60Pb40 and Sn41Bi57Ag2, are soldered on the front side busbars of industrial, mono-crystalline, screen-

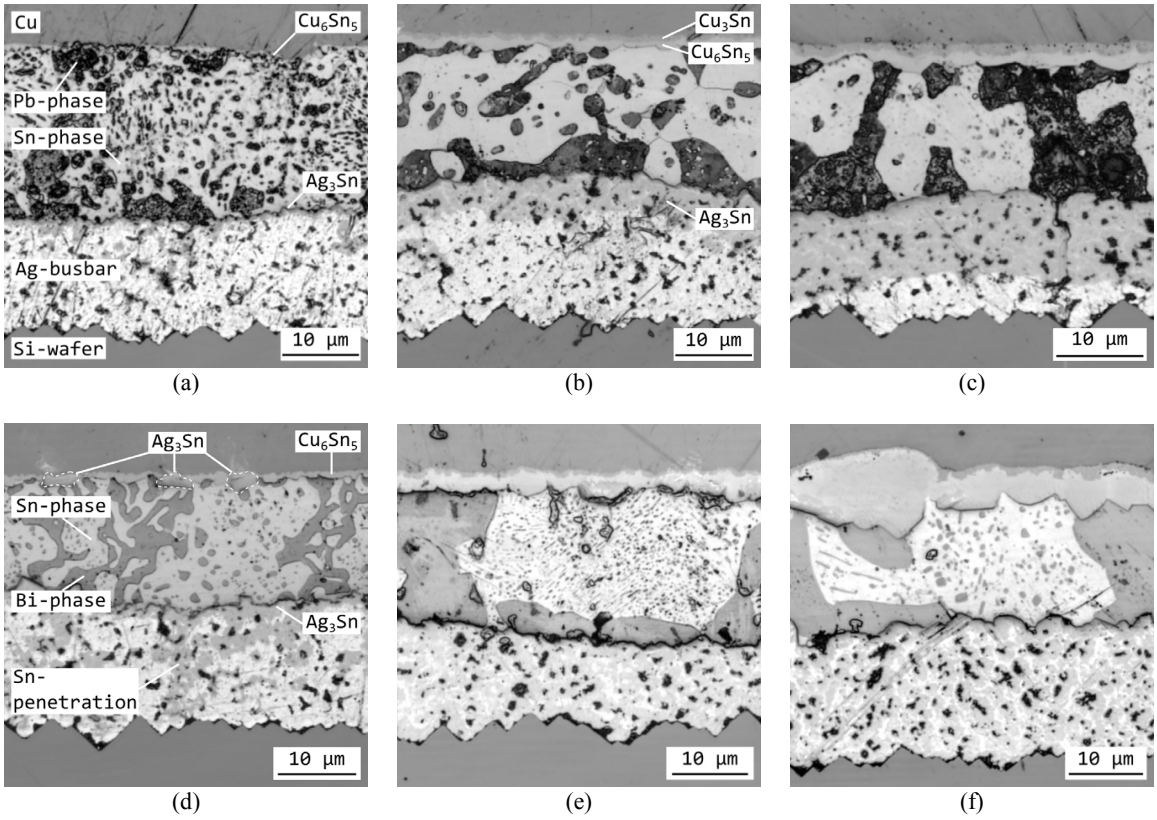

Figure 2. (a) CLM image of Sn60Pb40 solder bond in the initial state, (b) after 155 h at 130 °C, (c) after 500 h at 130 °C. (d) Sn41Bi57Ag2 solder bond in the intial state, (e) after 155 h at 130 °C, (f) after 500 h at 130 °C.

printed aluminium back-surface-field solar cells by means of a semi-automatic soldering station (Figure 1). The ribbon properties and process parameters are given in Table I.

Afterwards, metallographic cross sections are prepared [31]. These cross sections are thermally aged in a furnace under nitrogen flow at four temperatures between 85 °C and 150 °C depending on the solder melting temperature. Aging the embedded cross section samples allows to characterize nearly the same position in the interconnection before and after the thermal treatment. The time intervals to log the IMC thickness are 15 h, 85 h and 155 h. Selected samples are monitored for 500 h and 750 h. Before the microscopic inspection the samples are mechanically polished.

The samples are characterized with confocal laser microscopy (CLM), scanning electron microscopy (SEM) and electron dispersive x-ray spectroscopy (EDX). The thickness of the IMC is determined by positioning 30 measurement lines perpendicular to the layer, which are distributed across the entire cross section. An average value and a standard error are calculated.

3 RESULTS AND DISCUSSION

3.1 Microstructural changes and IMC growth

The metallographic cross section of the Sn60Pb40 solder bond in the initial condition is shown in Figure 2a. It is observed that Sn and Pb crystals with a diameter of 1 µm to 10 µm are uniformly distributed within the solder matrix. Occasionally, small sized Sn regions enclosed by Pb grains are found resulting from the secondary crystallization of Sn during the cooldown [10]. A Cu_6Sn_5 intermetallic layer with a thickness of 0.3 µm to 0.5 µm is found at the interface to the copper ribbon, which has a scallop-type morphology [32]. Between solder matrix and Ag-busbar there exists an Ag_3Sn intermetallic layer with a thickness of ≈0.7 µm. This layer is usually uniform, but excessive soldering temperature or time may lead to plate-like protrusions [14,33]. There are dark gray areas in the upper region of the busbar often located around lead-glass particles or cavities (black regions). These areas are afflicted with local Sn-penetration as will become evident in section 3.2.

After 155 h of thermal aging at 130 °C shown in Figure 2b, we find the grains of Sn and Pb to coarsen to diameters between 10 µm to 30 µm. Furthermore, in some locations fine cracks between the grains are identified. The IMC layers show notable growth after the thermal treatment. First, an intermediate IMC between Cu_6Sn_5 and Cu is formed, which is Cu_3Sn with a thickness of ≈0.3 µm. The Cu_6Sn_5 IMC measures between 1 µm to 1.5 µm. At the interface to the busbar the Ag_3Sn layer increases to 4 – 6 µm. Sn-penetration proceeds in such a way that it almost reaches the wafer surface.

The microstructure after 500 h at 130 °C shows further grain coarsening and IMC growth. The Ag-busbar is largely consumed by Ag_3Sn with a thickness of 10 – 12 µm. The total busbar thickness is 15 µm.

The initial state of the Sn41Bi57Ag2 solder bond is depicted in Figure 2d. The Bi and Sn grains are homogeneously dispersed in the solder matrix in a similar manner as in the case of Sn60Pb40. We measure that Cu_6Sn_5 and Ag_3Sn layer thicknesses are slightly higher with 0.6 µm and 0.8 – 0.9 µm respectively. The Ag-content in the solder matrix is largely found as Ag_3Sn clusters with 1 – 2 µm in diameter beaded at the interface to the Cu ribbon. Moreover, small Bi grains with a diameter of < 2 µm are distributed in the larger Sn grains. Furthermore, areas with Sn penetration extend in the busbar with up to 5 – 10 µm locally.

Thermal aging proceeds faster in the Sn41Bi57Ag2 solder joint as shown in Figure 2e. Notably, the Bi and Sn grains coarsen to form large, continuous clusters. However, the initially existent, small-sized Bi particles in the Sn grains now appear to form an even more finely grained matrix, whereby the diameters of the Bi grains are below 1 µm. The Cu_6Sn_5 layer is 2 µm to 3 µm and the Cu_3Sn ≈1 µm. We observe the Ag_3Sn to fill the entire busbar already after 155 h of thermal aging at 130 °C.

The effects of further ripening of the Sn41Bi57Ag2 bond become obvious in Figure 2f. After 500 h at 130 °C thermal aging, the IMCs possess an excessive thickness. The Cu_6Sn_5 phase reaches a thickness of 8 – 10 µm. It is observed that in some samples, especially when the solder layer is thin (5 – 10 µm), the solder matrix is practically depleted of Sn with only the Bi component remaining. This circumstance is assumed to cause a reduced fatigue life of the joint due to the brittleness of Bi, which is not able to absorb high mechanical stress without crack initiation. Judging from these microstructural observations we suspect lower reliability of Sn41Bi57Ag2 joints compared to standard Sn60Pb40 solder joints.

The development of the IMC thickness with time and temperature is shown in Figure 3. The experimentally determined thickness with CLM is plotted as symbols. Simulations according to the approach proposed in section 2.2 are shown as lines. The IMC thickness of Cu_6Sn_5 and Cu_3Sn at the Cu interface of the Sn41Bi57Ag2 solder bond is combined to a single phase growth. The reason is that Cu_3Sn can grow in expense of Cu_6Sn_5 in some instances as reported in reference [34], which leads to a stagnation of the Cu_6Sn_5 thickness. In turn, this stagnation strongly increases the error during the extraction of the activation energy, which is why we decide to simplify the IMC growth for this solder and IMC to a combined Cu_6Sn_5 + Cu_3Sn growth.

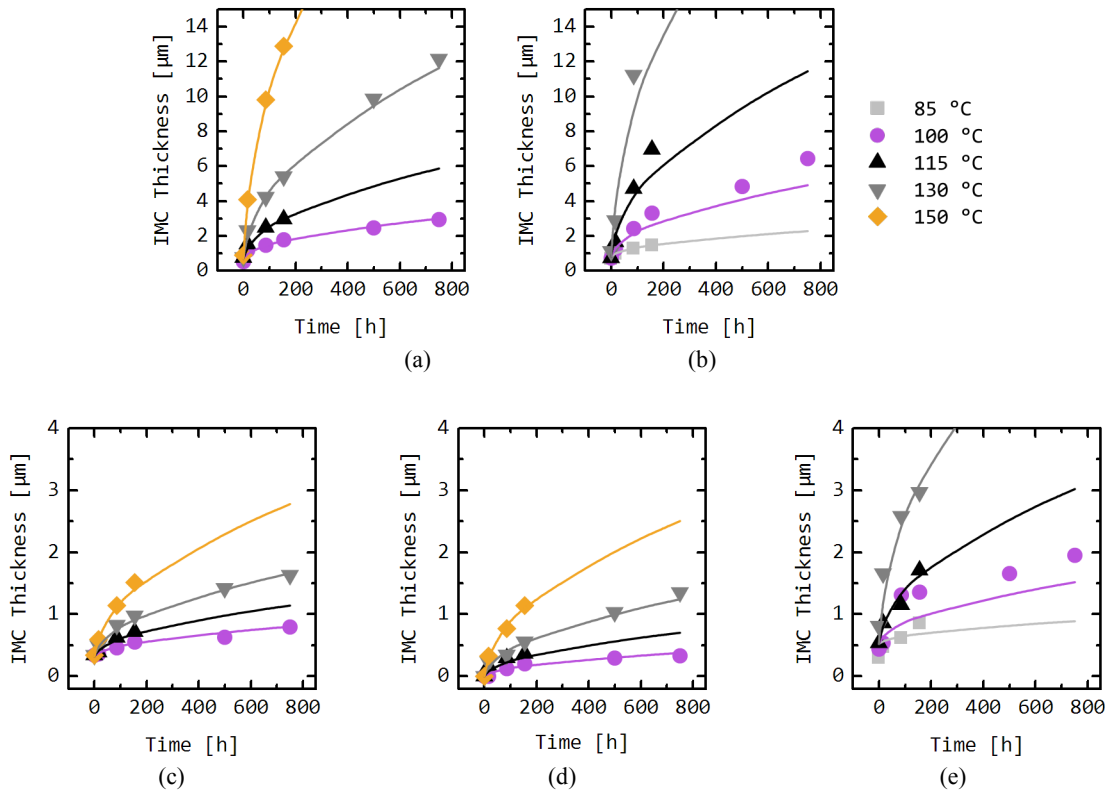

Figure 3. (a) Growth of Ag_3Sn in Sn60Pb40 solder bonds at different aging conditions, b) Ag_3Sn / Sn41Bi57Ag2, c) Cu_6Sn_5 / Sn60Pb40, d) Cu_3Sn / Sn60Pb40, e) Cu_6Sn_5 + Cu_3Sn / Sn41Bi57Ag2. Symbols represent measurements, lines represent simulated phase growth. Adapted from reference [38].

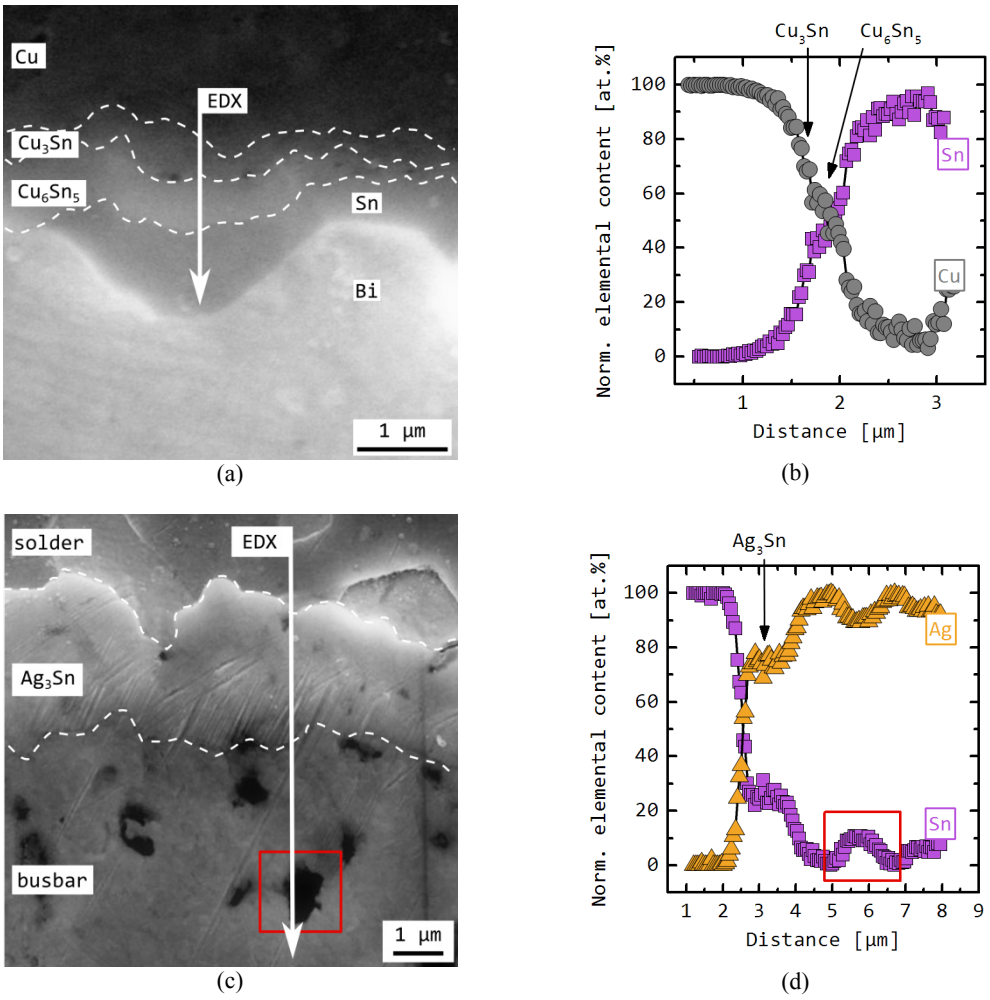

Figure 4. (a) SEM of the interface to the Cu ribbon of a Sn41Bi57Ag2 joint aged at 100 °C for 155 h, (b) EDX line scan across the interface that is shown in (a), (c) SEM of the interface from Sn41Bi57Ag2 to the busbar after 85 h at 100 °C. The red rectangle highlights a cavity in the busbar, (d) EDX line scan of the interface that is shown in (c). Adapted from references [38,39].

3.2 EDX analysis of the interfaces

The intermetallic layers at the interfaces are investigated in more detail using SEM and EDX techniques. A SEM detail of the interface at the Cu ribbon is depicted in Figure 4a. Both intermetallic phases appear as relatively uniform layers. An arrow indicates the range of a quantitative EDX line scan across this interface, which is shown in Figure 4b. The normalized elemental content in at.% of only the elements Sn and Cu is plotted versus the distance across the interface. In the region of Cu_6Sn_5 an elemental content of 40 at.% to 60 at.% Cu and respective Sn is found, which is close to the theoretically predicted content of 54.55 at.% Cu and 45.45 at.% Sn.

The Cu_3Sn phase is more difficult to verify with EDX, since no distinct plateau, where the elemental content would match the theoretically predicted 75 at.% Cu and 25 at.% Sn can be identified in the line scan. However, this is due to limitations in the resolution of the measurement.

Figure 4c shows a SEM detail of the Ag3Sn layer of a Sn41Bi57Ag2 solder bond aged 85 h at 100 °C and Figure 4d the EDX line scan across this interface accordingly. The red rectangle marks a special area of interest, which is a cavity in the busbar. The EDX line scan shows a plateau at the region of the Ag_3Sn intermetallic layer. There, an elemental content of 70 at.% to 75 at.% Ag and 25 at.% to 30 at.% Sn is determined, that is close to the theoretical stoichiometric ratio of the IMC. Unexpectedly, a significant amount of Sn is found around the cavity in the busbar highlighted by the red rectangle. Approximately 90 at.% Ag and 10 at.% Sn is measured in this region, which is assumed to be, according to the phase diagram, either (ζAg) or (Ag) with up to 10 at.% Sn in solid solution [17]. This finding corresponds to the gray areas around the cavities in the microscopic images that were mentioned in section 3.1 and interpreted as Sn- penetration. Therefore, we conclude that Sn is present in deeper regions of the busbar. It is likely that defects and cavities in the busbar promote the diffusion of Sn atoms from the solder into the busbar. Sn-penetration is often proposed as the reason for metallization adhesion loss after soldering or prolonged aging [35,36]. Therefore, this phenomenon is regarded as critical for interconnection reliability.

3.3 Simulation of IMC growth

The measured IMC thickness is converted to Arrhenius

plots according to equation 4. An example is provided for the case of Ag_3Sn using Sn41Bi57Ag2 in Figure 5. Theoretically, the three time series should result in the same slope, ergo activation energy, if a single reaction type and an independency of the activation energy on the progress of reaction is assumed. Obviously, the slopes of time series 85 h and 155 h are parallel, and the 15 h time series shows some deviation, which is similarly found in other cases. The reason for this deviation could be rooted in another kind of chemical reaction besides diffusion such as a phase-boundary or interface controlled process that is dominant in these early stages of ripening [37]. For practical reasons a weighted average of the slopes is taken in order to extract a single activation energy of the process. The activation energies and pre-exponential factors are reported in reference [38,39].

The quality of prediction of the simulation is quantified with the mean absolute error (MAE) between simulated data and experimental data [40]. In most cases a MAE < 1 µm is obtained indicating a good predictability.

The kinetic parameters are used to calculate the phase growth that we assume to occur during PV module reliability tests thermal cycling from –45 °C to 85 °C (TC) and a constant temperature of 85 °C, as present in damp heat tests [41]. The predicted IMC growth after TC 600 (cycles) with a cycle time of 2.8 h is shown in Figure 6a. For the Ag_3Sn layer a thickness of 1.5 µm with Sn41Bi57Ag2 and 1.2 µm with Sn60Pb40 is calculated. Owing to the extended time periods at low temperatures during this test the IMC thickness remains quite limited.

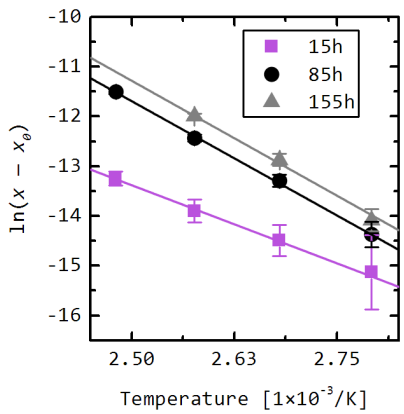

Figure 5. Arrhenius plot of the Ag3Sn growth using Sn41Bi57Ag2 solder. Adapted from reference [38].

The result for 3000 h at a constant temperature of 85 °C is shown in Figure 6b. Note that any possible effects of humidity are not included in the calculation. After 3000 h an Ag_3Sn thickness for Sn41Bi57Ag2 of 3.7 µm compared to 2.6 µm for Sn60Pb40 is calculated. The results indicate that a notable phase growth takes place during a constant temperature treatment of 85 °C.

Furthermore, the model is applied to make a prognosis of the phase growth within a PV module in an outdoor location. Module temperature data of a crystalline silicon PV module installed in Freiburg, Germany is chosen. The temperature curve over the course of one year recorded at one hour time intervals is shown in Figure 7a. This temperature curve is iterated 25 times in the numerical algorithm to simulate a module life of 25 years.

The progression of the Ag_3Sn phase using Sn60Pb40 during the first year is shown in Figure 7b. Since the temperature measurement starts in the summer period, the phase growth is initiated rapidly, slows down in winter and reoccurs in spring the following year. Thus, the phase growth is described as a step-wise increase each year. The prognosis for 25 years is shown in Figure 7c, where this step-wise increase becomes apparent over a longer time scale. Globally, the curve still follows a parabolic shape as consequential from the theoretical background. Surprisingly, a very limited Ag_3Sn phase growth after 25 years of only 1.3 µm and 1.2 µm for Sn41Bi57Ag2 and Sn60Pb40 is calculated respectively. This is, however, plausible if it is considered that the module temperature rarely exceeds 60 °C. Due to the relatively high activation energy of the process, phase growth becomes very slow at these temperatures compared to thermal aging at elevated temperatures. PV modules installed in desert climates can, of course, show a stronger intermetallic phase growth.

The proposed model is able to make predictions of the IMC growth even for non-uniform temperature profiles, which occur in real outdoor conditions and is therefore highly applicable in practice. Judging from the forecasts based on temperature profiles of typical

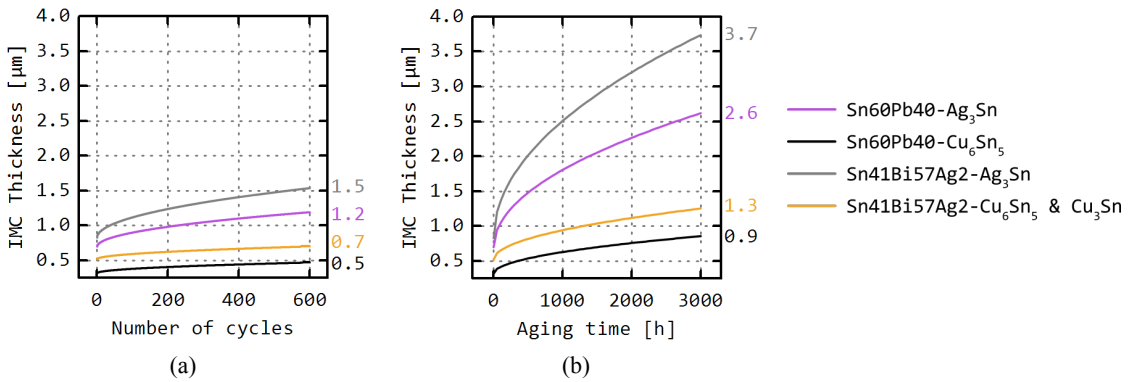

Figure 6. (a) Simulated phase growth of a PV module in a thermal cycling test, (b) simulated phase growth during constant 85 °C. Adapted from references [38,39].

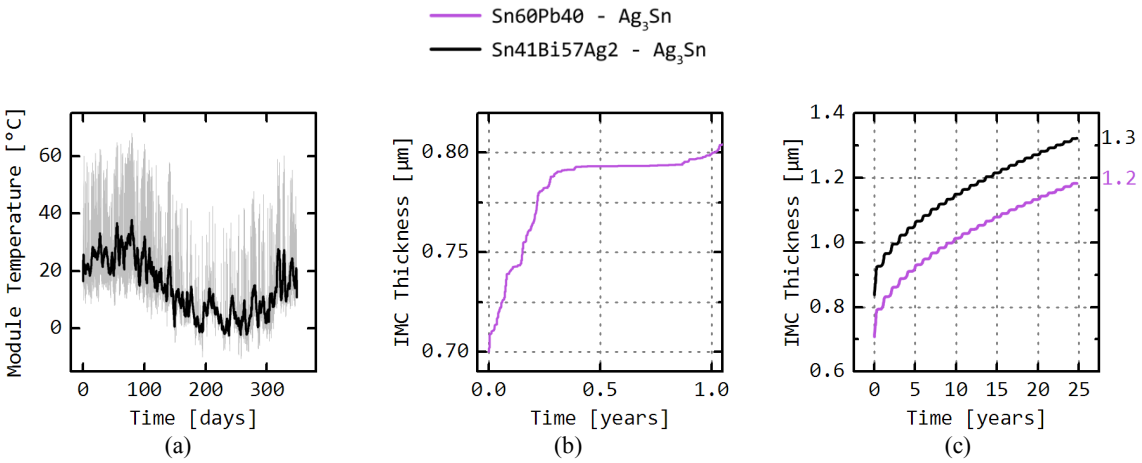

Figure 7. (a) Development of the module temperature during one year (June 01, 2012 to May 15, 2013) in Freiburg, Germany. The gray curve is temperature data recorded at a one-hour intervals. The black curve is a floating average for easier readability. (b) Predicted IMC growth of Ag_3Sn using Sn60Pb40 during the course of the first year. (c) Predicted IMC growth during the course of 25 years. Adapted from references [38,39].

accelerated aging tests and an outdoor location, it is assumed that phase growth directly at the interfaces is rather limited in many situations. Additionally, the differences between Sn41Bi57Ag2 and standard Sn60Pb40 are estimated to be not large. Probably, other observed aging mechanisms such as grain coarsening of the solder matrix or Sn-penetration may be dominant factors having an impact on reliability. Supplementary reliability tests of Sn41Bi57Ag2 soldered PV modules and outdoor testing need to be done in order to further evaluate the potential of the material.

5 CONCLUSION

The microstructure and IMC growth of Sn60Pb40 as well as Sn41Bi57Ag2 solder joints is studied. The uniform and thin IMCs formed during the soldering process at the interfaces to the Cu ribbon and the cell metallization indicate stable metallurgical bonds. They are 0.3 – 0.6 µm and 0.7 – 0.9 µm in thickness for Cu_6Sn_5 and Ag_3Sn respectively. However, it is confirmed with EDX that dissolved Sn exists around cavities in the busbar already in the as-soldered condition. Furthermore, it is observed that IMC growth and other ripening processes during thermal aging such as grain coarsening and Sn-penetration proceed faster in Sn41Bi57Ag2 solder joints owing to the high homologous temperature of the material in many situations. In particular, an entire consumption of the busbar by Ag_3Sn is found after relatively short aging times of 155 h at 130 °C, and in some cases even a depletion of Sn in the solder matrix with only Bi remaining after 500 h for the Sn41Bi57Ag2 solder. The observed ripening processes are assumed to cause commonly observed reliability problems such as metallization adhesion loss and a reduction of fatigue life.

The kinetics of IMC growth are described by a model based on diffusion. The model is parameterized by the Arrhenius approach and the necessary systematic thermal aging experiments. A good predictability of MAE < 1 µm in many cases is achieved.

The model is applicable to many practical situations including non-isothermal temperature conditions and allows the development of customized accelerated aging tests. Examples for model application to predicting the phase growth during accelerated aging tests of PV modules results in 1.2 µm for Ag_3Sn in Sn60Pb40 bonds and 1.5 µm for Ag_3Sn in Sn41Bi57Ag2 joints after TC 600. Furthermore, 2.6 µm of Ag_3Sn in Sn60Pb40 and 3.7 µm of Ag_3Sn in Sn41Bi57Ag2 after 3000 h at 85 °C are predicted. Eventually, a prognosis of phase growth during 25 years of module life in the outdoor location Freiburg, Germany leads to a final thickness of 1.2 µm for Ag_3Sn using Sn60Pb40 and 1.3 µm using Sn41Bi57Ag2.

REFERENCES

[1] M.A. Green, Nat. Energy 1 (2016), 1–4.
[2] T. Geipel, J. Moeller, Y. Zemen, S. Pingel, J. Berghold, Proceedings of the 26th European Photovoltaic Solar Energy Conference and Exhibition (2011), 3517–3522.
[3] J. Wendt, M. Träger, M. Mette, A. Pfennig, B. Jäckel, Proc. of the 24th EUPVSEC. 24th EUPVSEC (2009), 2705–2708.
[4] A.M. Gabor, Proceedings of the 21st European Photovoltaic Solar Energy Conference and Exhibition (2006), 2042–2047.
[5] D.L. King, M.A. Quintana, J.A. Kratochvil, D.E. Ellibee, B.R. Hansen, Prog Photovoltaics 8 (2000), 241–256.
[6] M.A. Quintana, D.L. King, T.J. McMahon, C.R. Osterwald, Proceedings of the 29th IEEE Photovoltaic Specialists Conference (2002), 1436–1439.
[7] G. Cuddalorepatta, A. Dasgupta, S. Sealing, J. Moyer, Tolliver, T.Loman, J., Prog Photovoltaics 18 (2010), 168–182.
[8] P.L. Tu, Y. Chan, J. Lai, IEEE Trans. Compon. Packag. Manuf. Technol. B 20 (1997), 87–93.
[9] A. Faes, M. Despeisse, J. Levrat, J. Champliaud, N. Badel, M. Kiaee, T. Söderström, Y. Yao, R. Grischke, M. Gragert, J. Ufheil, P. Papet, B. Strahm, G. Cattaneo, J. Cattin, Y. Baumgartner, A. Hessler-Wyser, J. Balliet, Proceedings of the 29th

European Photovoltaic Solar Energy Conference and Exhibition (2014), 2555–2561.
[10] Klein Wassink, R. J. Weichlöten in der Elektronik [Soldering in Electronics], 2nd ed., Leuze, Saulgau/Württ (1991).
[11] T. Laurila, V. Vuorinen, J.K. Kivilahti, Materials Science and Engineering: R: Reports 49 (2005), 1–60.
[12] P.G. Harris, K.S. Chaggar, M.A. Whitmore, Soldering & Surface Mount Tech 3 (1991), 20–33.
[13] Parent, J. O. G., Chung, D. D. L., I.M. Bernstein, J Mater Sci 23 (1988), 2564–2572.
[14] K. Zeng, K.N. Tu, Materials Science and Engineering: R: Reports 38 (2002), 55–105.
[15] D.R. Frear, P.T. Vianco, Metall and Mat Trans A 25 (1994), 1509–1523.
[16] N. Saunders, A.P. Miodownik, Bulletin of Alloy Phase Diagrams 11 (1990), 278–287.
[17] I. Karakaya, W.T. Thompson, Bulletin of Alloy Phase Diagrams 8 (1987), 340–347.
[18] Official Journal of the European Union, Directive 2011/65/EU of the European Parliament and of the Council of 8 June 2011 on the restriction of the use of certain hazardous substances in electrical and electronic equipment (recast) (2011).
[19] B. Lalaguna, P. Sánchez-Friera, I.J. Bennett, D. Sánchez, L.J. Caballero, Alonso J., Proceedings of the 22nd European Photovolatic Solar Energy Conference and Exhibition (2007), 2712–2715.
[20] B. Lalaguna, P. Sánchez-Friera, H. Mäckel, D. Sánchez, J. Alonso, Proceedings of the 23rd European Photovoltaic Solar Energy Conference and Exhibition (2008), 2705–2708.
[21] M. Mccormack, H.S. Chen, G.W. Kammlott, S. Jin, Journal of Elec Materi 26 (1997), 954–958.
[22] W.-R. Myung, M.-K. Ko, Y. Kim, S.-B. Jung, J Mater Sci: Mater Electron 26 (2015), 8707–8713.
[23] M.J. Burek, S. Jin, M.C. Leung, Z. Jahed, J. Wu, A.S. Budiman, N. Tamura, M. Kunz, T.Y. Tsui, Acta Materialia 59 (2011), 4709–4718.
[24] P.L. Liu, J. Shang, Scripta Materialia 53 (2005), 631–634.
[25] X. Hu, Y. Li, Z. Min, J Mater Sci: Mater Electron 24 (2013), 2027–2034.
[26] K. Suganuma, Current Opinion in Solid State and Materials Science 5 (2001), 55–64.
[27] Z. Mei, J. Morris, JEM 21 (1992), 599–607.
[28] R. Strauss, S. Smernos, Circuit World 10 (1984), 23–25.
[29] L.E. Felton, C.H. Raeder, D.B. Knorr, JOM 45 (1993), 28–32.
[30] R.J. Borg, G.J. Dienes An Introduction to Solid State Diffusion, Academic Press, San Diego (1988).
[31] D. Eberlein, P. Schmitt, P. Voos, Practical Metallography 48 (2011), 239–260.
[32] H.K. Kim, H.K. Liou, K.N. Tu, Appl. Phys. Lett. 66 (1995), 2337.
[33] P.T. Vianco, R.D. Wright, P.F. Hlava, J.J. Martin, Metall and Mat Trans A 37 (2006), 1551–1561.
[34] A.C.K. So, Y.C. Chan, J. Lai, IEEE Trans. Comp., Packag., Manufact. Technol. B 20 (1997), 161–166.
[35] P. Schmitt, P. Kaiser, C. Savio, M. Tranitz, U. Eitner, Enrgy Proced 27 (2012), 664–669.
[36] W.A. Crossland, L. Hailes, Solid State Technology (1971), 42–47.
[37] J. Šesták, G. Berggren, Thermochimica Acta 3 (1971), 1–12.
[38] T. Geipel, M. Moeller, A. Kraft, U. Eitner, Sol Energ Mat Sol C (submitted).
[39] T. Geipel, M. Moeller, A. Kraft, U. Eitner, Energy Procedia (submitted).
[40] D.G. Mayer, D.G. Butler, Ecological Modelling 68 (1993), 21–32.
[41] IEC 61215: 2005-04, Crystalline silicon terrestrial photovoltaic (PV) modules - Design qualification and type approval (2005).